Research Square

Preprints are preliminary reports that have not undergone peer review.
They should not be considered conclusive, used to inform clinical practice,
or referenced by the media as validated information.

A near-certain late-summer drought hotspot across southern and eastern Europe under global warming

Henri Funk

henri.funk@lmu.de

Ludwig-Maximilians-Universität München https://orcid.org/0009-0007-0949-8385

Alexander Sasse

Ludwig-Maximilians-Universität München

Andrea Böhnisch

Ludwig-Maximilians-Universität München

Cornelia Gruber

Ludwig-Maximilians-Universität München https://orcid.org/0009-0002-0657-3558

Ralf Ludwig

Ludwig-Maximilians-Universität München

Helmut Küchenhoff

Ludwig-Maximilians-Universität München https://orcid.org/0000-0002-6372-2487

Magdalena Mittermeier

Ludwig-Maximilians-Universität München https://orcid.org/0000-0002-8668-281X

Research Article

Keywords:

Posted Date: August 12th, 2026

DOI: https://doi.org/10.21203/rs.3.rs-10585537/v2

License: This work is licensed under a Creative Commons Attribution 4.0 International License.
Read Full License

Additional Declarations: The authors declare no competing interests.

A near-certain late-summer drought hotspot across southern and eastern Europe under global warming

Henri Funk[1,2,3,*], Alexander Sasse[2], Andrea Böhnisch[2], Cornelia Gruber[4], Ralf Ludwig[2], Helmut Küchenhoff[1], and Magdalena Mittermeier[2]

[1]Statistical Consulting StaBLab, LMU Munich, Munich, Germany
[2]Department of Geography, LMU Munich, Munich, Germany
[3]Munich Center for Machine Learning, MCML, Munich, Germany
[4]Department of Statistics, LMU Munich, Munich, Germany

[*]Author to whom any correspondence should be addressed. E-mail: H.Funk@lmu.de

Abstract. Drought poses a major threat to agriculture, water supply, and ecosystems in Europe. Regional climate model projections provide future scenarios and internal variability, an irreducible uncertainty, essential to assess drought risk under global warming. Here, we reveal that under +3 °C global warming, isolated drought clusters are near-certain to merge into a single southeastern hotspot. By constructing variability bounds on the Standardized Precipitation Evapotranspiration Index of a regional single-model large ensemble, we show that climate shifts into a drier state in which the Iberian Peninsula, the Mediterranean, and Eastern Europe are almost certain to face a recurrent, large-scale drought hotspot. Mountain ranges mark the boundary between this hotspot and the wetter northern continent. Nevertheless, the area covered by local drought hotspots in the North increases sharply under +3 °C of global warming. Increasing variability across most drought hotspots indicates that amplified and possibly unprecedented extremes are likely to emerge.

Introduction

Drought ranks among the most damaging and evolving climate hazards affecting Europe, with consequences that reach across agriculture, water supply, energy production, ecosystems, transportation, and public health [1, 2, 3, 4]. The past two decades delivered a sequence of exceptional events. The 2003 heat and drought, the consecutive dry summers of 2018 and 2019, and the widespread 2022 drought each produced record water deficits and severe socioeconomic losses across large parts of the continent [5, 6]. Europe has emerged as a hotspot of intensifying heat [7]. Projections under continued warming point to a strengthening of the south-west to north-east contrast, with more frequent and more severe drought across western Europe and the Mediterranean, and milder change or wetting in the north [2, 8].

Drought frequently coincides with extreme heat, forming compound hot and dry events whose combined impact exceeds the sum of the individual hazards [9, 10, 11]. These events typically develop under persistent high-pressure systems through thermodynamic land–atmosphere coupling and positive feedbacks that amplify and sustain the heat [12, 7].

The Standardized Precipitation Evapotranspiration Index (SPEI) has become the reference index for meteorological droughts in Europe [13]. It responds to the heat-driven moisture loss associated with these compound events, as well as to precipitation deficits, by relying on the potential water budget over a specified aggregation period (e.g., 1-12 months). Across Europe, the SPEI signal exhibits drying as warming increases evaporative demand and expands the area under drought [14]. Under future warming, it projects drying over a far greater fraction of land than purely precipitation-based indices [15].

The current seasonal climatology, depicted in Figure 1, already shows a strong, seasonally varying gradient across Europe, with wet winter and spring conditions giving way to a pronounced summer. Values below -1 and -1.5 are classified as moderate and severe droughts, respectively [13, 16].

Projecting how these conditions evolve under global warming is limited by the internal variability of the climate system, which dominates the uncertainty of regional drought projections [17, 18, 19]. Single-model initial-condition large ensembles provide the necessary data to robustly quantify this component [20, 21, 22]. When assessing drought trends for each member separately, the resulting spread represents internal variability, ranging from the wettest (best-case) estimate within the ensemble to the driest (worst-case) estimate. Internal variability in large ensembles has usually been quantified as the inter-member spread inside fixed multi-decadal windows [23, 24].

Treated as an aleatoric, hence irreducible, uncertainty, internal variability becomes a quantity that can be estimated [25, 26, 27]. We propose a novel method to estimate spatio-seasonal variability as a smooth function of the forced climate state, yielding a continuous, window-free drought trajectory and, for the first time, a 95% confidence interval for the SPEI-3, whose wet end sets the minimum drought exposure Europe can expect under global warming. This minimum state of drought exposure can also be interpreted as near-certain under the given level of global warming. To obtain this near-certain case, we extend the aleatoric-uncertainty decomposition of

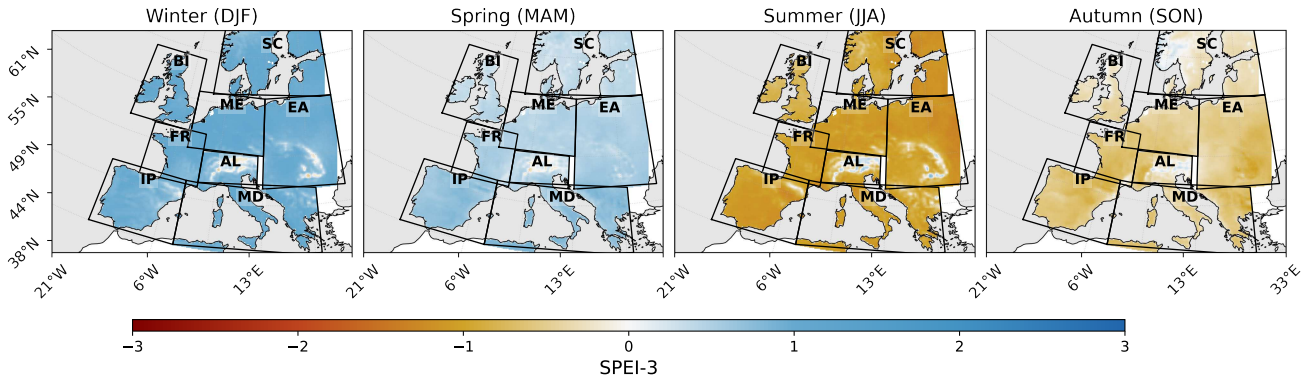

Figure 1. Seasonal drought index over Europe derived from ERA5-Land (1971–2020), shown for winter (DJF), spring (MAM), summer (JJA), and autumn (SON). The eight PRUDENCE region boundaries are overlaid and classified, spanning the British Isles (BI) in the north-west and Scandinavia (SC) in the north, France (FR) and the Iberian Peninsula (IP) in the west and south-west, Mid-Europe (ME) and the Alps (AL) across the central interior, the Mediterranean (MD) along the southern seaboard, and Eastern Europe (EA) to the east. Values represent the time mean of the seasonally aggregated SPEI-3. The colour scale runs from strongly negative, indicating drought-prone conditions, to strongly positive, indicating wet-prone conditions.

Gruber et al. [25] across the eight European PRUDENCE regions [28], as shown in Figure 1. Here, expected drought trends and variability are assessed under global warming and compared with present conditions using fixed 20-year windows defined around global warming levels (GWL) of present (PRES: near +1.2 °C), GWL2: +2 °C, and GWL3: +3 °C [1, 29, 30].

The probabilistic bounds constructed from internal variability are compared across regions and global warming levels, aiming to answer the following research questions:

1. Which regions move recurrently into drought as global warming rises from the present to +2 °C and +3 °C, and how far does the forced SPEI signal shift?
2. How do the spatial and seasonal patterns of SPEI variability change, and how does the shifting variability interact with drought hotspots?
3. Where does the wet bound of the SPEI-3 variability interval fall below a drought threshold, indicating seasonal and regional drought exposure that can be expected to be almost certain under a given GWL?

Results

Droughts expand westwards and intensify under +3 °C

Using the SPEI-3 signal extracted from the large ensemble, we show that summer drying intensifies substantially across southern, western, and eastern Europe under GWL3 in the lower panel of Figure 2, but is greatly reduced when global warming is limited to +2 ° degrees in the middle panel. The already-dry hotspots expand substantially relative to present conditions in the upper panel of Figure 2. Drought hotspots under GWL3 encompass large regions in central Spain, the Mediterranean coast south of the Alps, and Turkey in summer [31]. This westward shift is essentially reduced under GWL2.

The GWL3 signal amplifies and extends the GWL2 patterns in all seasons. Europe shows a wetting signal in winter and spring in all regions but the Iberian Peninsula. This might relate to the annual decline of precipitation on the Iberian Peninsula under global warming [32]. In autumn, the spatial footprint of drying expands northward into northern France and the British Isles compared to GWL2. This intensification of seasonal drying characteristics aligns with projected precipitation trends in the CRCM5-LE [32]. Under GWL3, the high-elevation hotspots in autumn expand considerably compared to GWL2.

Figure 2 further indicates that under present conditions, drought is most pronounced in summer, with a secondary concentration in the south-east during autumn. Winter and spring are wet in most of Europe. The inner Alpine dry zone is the main exception, with dry conditions year-round [33]. Drought also occurs in eastern Europe around mountain ranges and in Scandinavia.

The drying signal under GWL2, in the middle row, is most pronounced in summer and autumn, with the strongest negative anomalies over eastern Europe, whereas the remaining regions show only moderate drying. The summer panel shows the clearest pattern. The already-dry hotspots under PRES (hatching in Figure 2, first row) extend under GWL2 from eastern Europe southwards to Greece and Turkey, and northwards into Scandinavia in summer, while isolated Alpine and Pyrenean high-elevation drought hotspots emerge in summer and autumn. Winter and spring show weak, spatially heterogeneous signals, with modest wetting over Scandinavia and parts of central Europe, and slight drying in the south.

Drought seasons are lengthening with ongoing global warming

In Figure 3, the drought season lengthens under global warming because the transition months between dry and wet seasons in each region are drying. Most regions experience

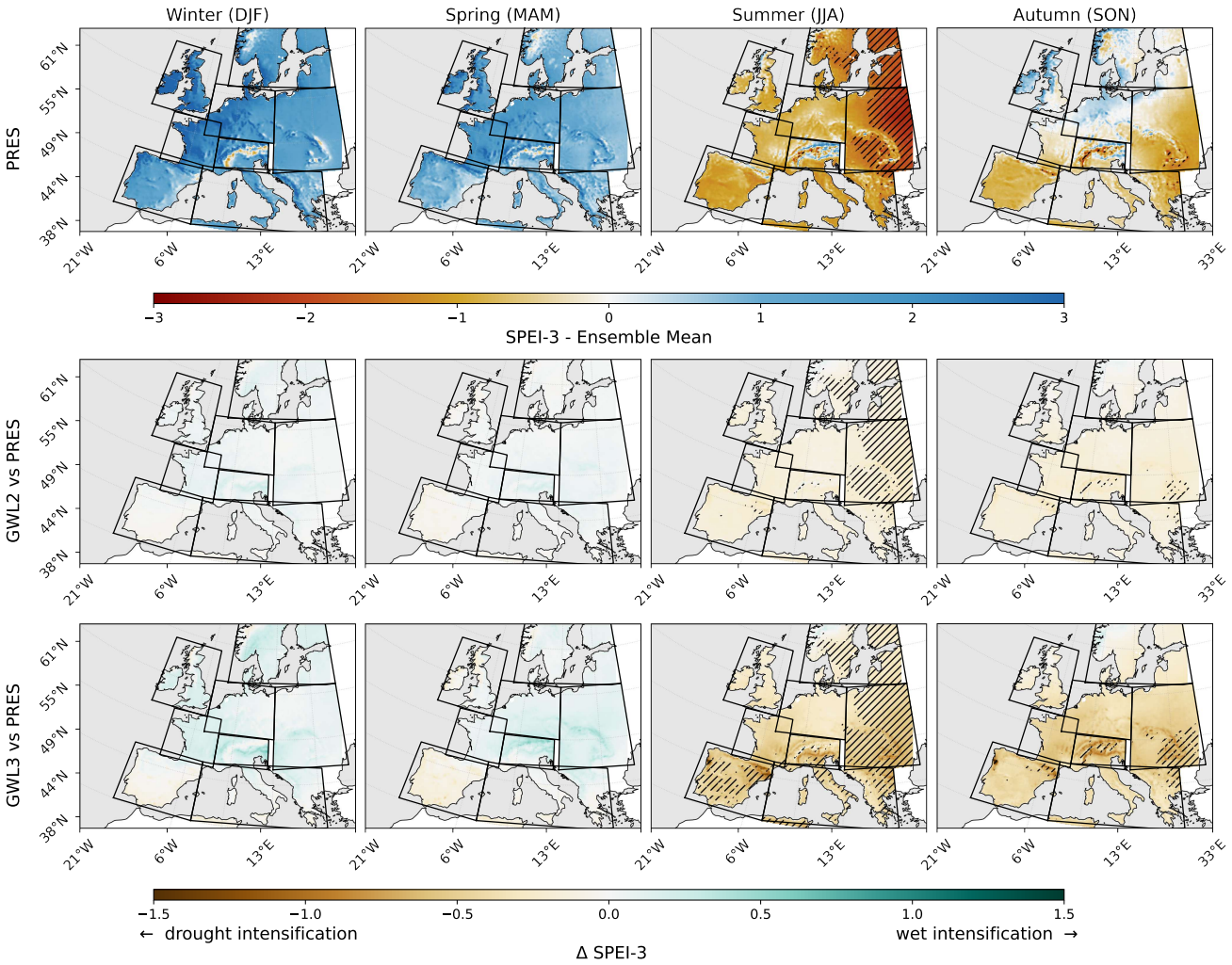

Figure 2. Expected seasonal drought index over Europe under present conditions in the upper row and change between each warming level and the present reference period for GWL2 in the mid row and GWL3 in the bottom row, across winter, spring, summer, and autumn. Hatching identifies grid cells in expected drought zones (SPEI-3 ≤ -1.5) under the given warming level.

two transitional months in which SPEI-3 is close to zero under present conditions, and these months increasingly show drought signals under global warming. Drought-prone months show a clear intensification in the SPEI signal, with a stable drier signal under global warming. The aggregated regions show weak wetting or no change in the wetter winter months. The less affected regions (BI, ME, AL) show three to four months under drought risk, while the most drought-prone regions (IP, MD, EA) show five months. Eastern Europe shows the strongest intensification of all regions under GWL3, with SPEI-3 reaching the most extreme drought values in Figure 3. The signal across almost all months and regions persists, with dry and wet signals only intensifying.

Summer SPEI-3 variability increases across most drought hotspots

Using the uncertainty framework [25], summer variability increases across most of Europe (third column in Figure 4), with the most pronounced trend under GWL3, affecting large parts of the continent. Most regions with increasing variability coincide with drought hotspots (see Figure 2), indicating synchronous increases in both drought intensity and variability. This underlines that amplified and potentially unprecedented extremes are likely to emerge [34, 35]. This risk is substantially reduced if global warming is limited to +2°C rather than +3°C. The pattern is not uniform, however: parts of the inner Iberian Peninsula and the Alpine core are exceptions, where variability decreases at drought hotspots as the dry regime stabilises. The Alpine region exhibits a distinct seasonal response: under GWL2, variability decreases around the Alps in autumn and north of the Alps in winter, whereas under GWL3, this reduction broadens across the central Alps in autumn, with localised increases restricted to high elevations.

The variability of the drought indicator changes markedly with ongoing global warming, showing an East-West divide in all seasons except summer. Under present conditions (top row, Figure 4), high SPEI-3 variability is dominated by orography and concentrates along the western coastline in autumn and spring, potentially driven by the interannual variability of the North Atlantic Oscillation (NAO) [36, 37]. Under continued

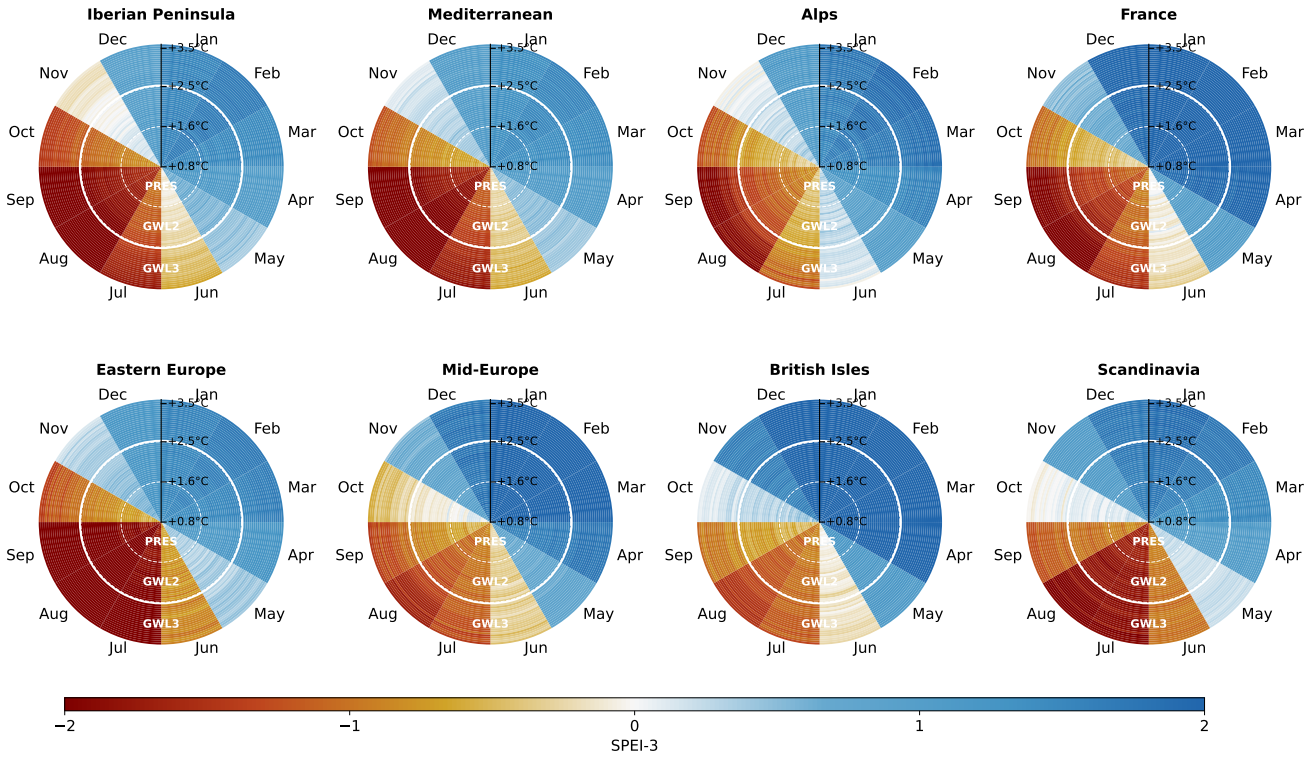

Figure 3. Radar plot showing expected monthly SPEI-3 responses under global warming, faceted by each PRUDENCE region. White rings indicate the borders between the GWL windows. Each ring represents the regional drought index for a given annual warming level by month.

warming, decreasing variability in western regions contrasts with increasing variability in the east, reinforcing this East-West pattern (see Figure 4).

Minimum drought-exposed land area expands across Europe under warming

The minimum land area under near-certain late-summer drought increases broadly across the European continent as warming proceeds (Figure 5). If warming continues to GWL3 (+3 °C), at least 60% of the Iberian Peninsula (IP) is almost certainly under drought in late summer. This guaranteed fraction is around 20% smaller when warming is limited to GWL2 (+2 °C). The near-certain fraction is an optimistic lower bound: it counts only the land where even the wettest plausible realisation of internal variability still produces drought, so it measures exposure to the near-certainly unavoidable drying at a given warming level. Figure 5 tracks the transient minimum within each yearly window, while Table 1 reports the corresponding 20-year window means.

For moderate drought (SPEI-3 ≤ -1.0), the Iberian Peninsula, the Mediterranean, and Eastern Europe are the most exposed, with 20-year GWL3 window means of about 60%, 52%, and 38% of regional land area, depicted in Table 1. Eastern Europe already carries a drought signal under present conditions, largely driven by rising temperatures [32, 38]. The Alpine domain and France respond very sensitively to GWL3. While the near-certain affected land fraction stays close to 0% under GWL2, it rises up to 25 to 50% at the end of GWL3 in Figure 5. The British Isles and Mid-Europe show no near-certain moderate drought in the window means, with only transient hotspots in individual GWL3 years.

Table 1. Mean SPEI-3 drought land area fraction (%) by PRUDENCE region and global warming level, for two drought thresholds.

	SPEI-3 ≤ -1.0			SPEI-3 ≤ -1.5		
Region	PRES	GWL2	GWL3	PRES	GWL2	GWL3
AL	0.0	0.1	5.3	0.0	0.0	0.1
BI	0.0	0.0	0.0	0.0	0.0	0.0
EA	15.0	24.0	37.8	2.3	7.2	18.2
FR	0.1	0.9	5.2	0.0	0.0	0.4
IP	21.1	37.4	59.8	0.1	4.5	22.4
ME	0.0	0.0	0.0	0.0	0.0	0.0
MD	14.7	28.8	52.2	0.3	3.5	17.4
SC	0.4	0.7	2.4	0.0	0.0	0.0

Severe drought (SPEI-3 ≤ -1.5) is led by Eastern Europe, the only region with noticeable near-certain severe exposure under present conditions, rising exponentially from around 2% of its land area at present to 7% at GWL2 and 18% at GWL3 (Table 1). By GWL3, the southern regions converge on comparable values, with the Iberian Peninsula reaching about 22% and the Mediterranean about 17%. The remaining regions (BI, ME, SC) carry little or no near-certain severe drought at any warming level.

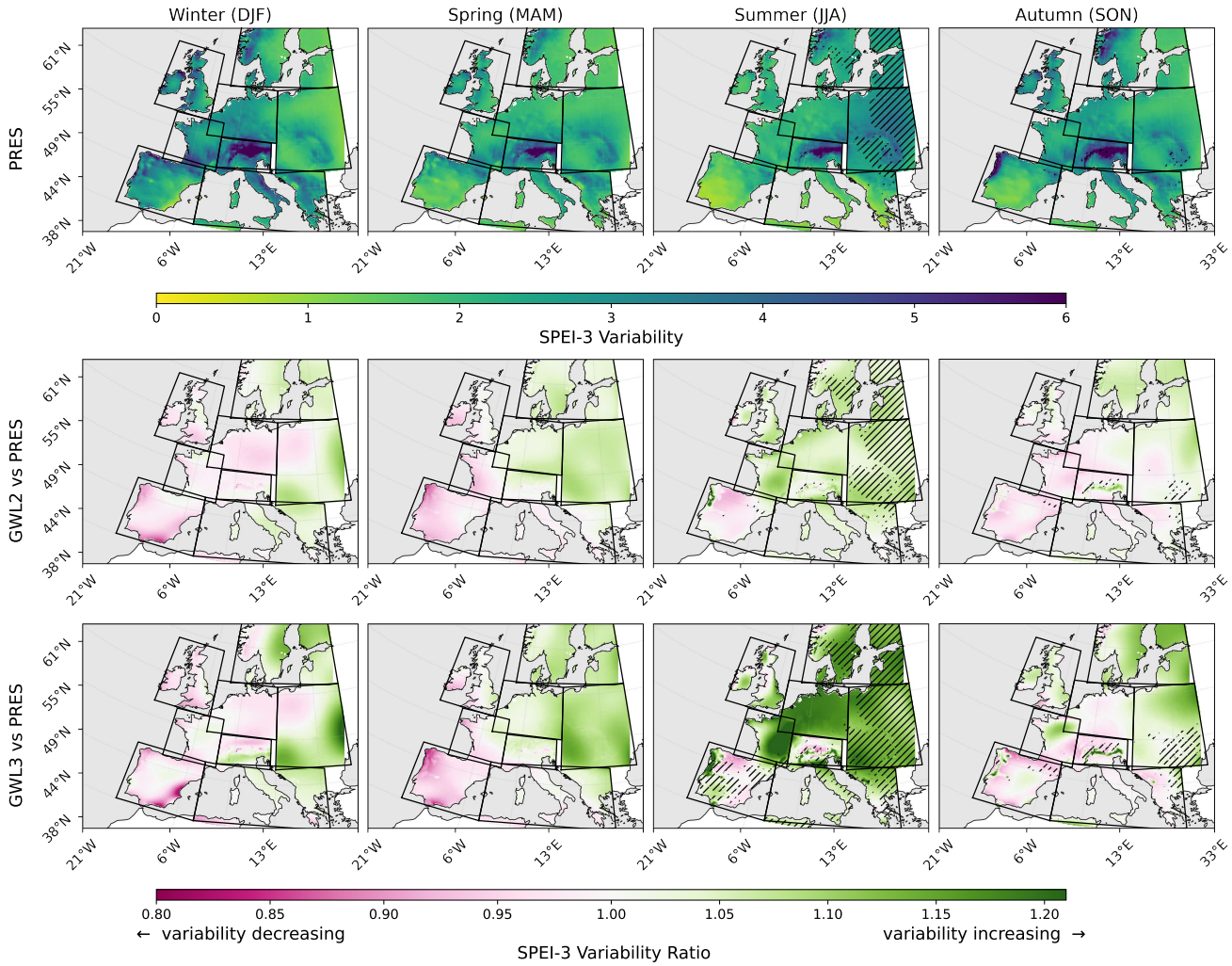

Figure 4. Expected seasonal SPEI-3 variability under present conditions (upper row) and ratio between each warming level and the present reference period for GWL2 (mid row) and GWL3 (bottom row), across winter, spring, summer, and autumn. Hatching identifies grid cells in expected drought zones (SPEI-3 ≤ -1.5) under the given warming level.

Recurrent late-summer drought hotspots merge under global warming

Encoding the minimal share of local drought exposure in late summers, Figure 6 indicates moderate drought hotspots in the Iberian Peninsula, along the Mediterranean coastline, and in Eastern Europe, merging into a single large-scale hotspot from the Iberian Peninsula along the Mediterranean coast up to Eastern Europe under GWL3. Even in an optimistic scenario, it yields late-summer droughts with a near-certain recurrence of 2 years ($\sim$ 50%). The severe drought hotspot indicates a similar but less persistent drought hotspot until GWL3 is reached. It can be expected to return at least every 3 years.

Two distinct hotspots are present under present warming for both moderate and severe drought conditions: the central Iberian Peninsula and Eastern Europe, including the Carpathian and Balkan ranges. IP and EA have a recurrence of $\sim$3 years for the moderate drought hotspot under wet conditions. The drought hotspots evolve and expand under global warming, primarily along Mediterranean coastlines. Visibly, the Pyrenees and central Spanish mountain ranges mark the boundary of drought exposure as it expands across the Iberian Peninsula. In line with these results, the Alps separate Mediterranean drought hotspots from the central and northern European landmass, and the eastern European mountain ranges could define the western boundary of the EA hotspot core.

Discussion

Across the full European climatological domain, the seasonal pattern under present conditions intensifies with global warming. Wet seasons, winter and spring become wetter. Dry seasons, summer and autumn become drier. Regional drought hotspots expand in summer and autumn. This seasonal divergence, with wetter winters and drier summers, reproduces the precipitation-only signal obtained for the same ensemble and multi-model projections [32, 8].

In every European region, the SPEI-3 drought season is centred around late summer. Under global warming, the

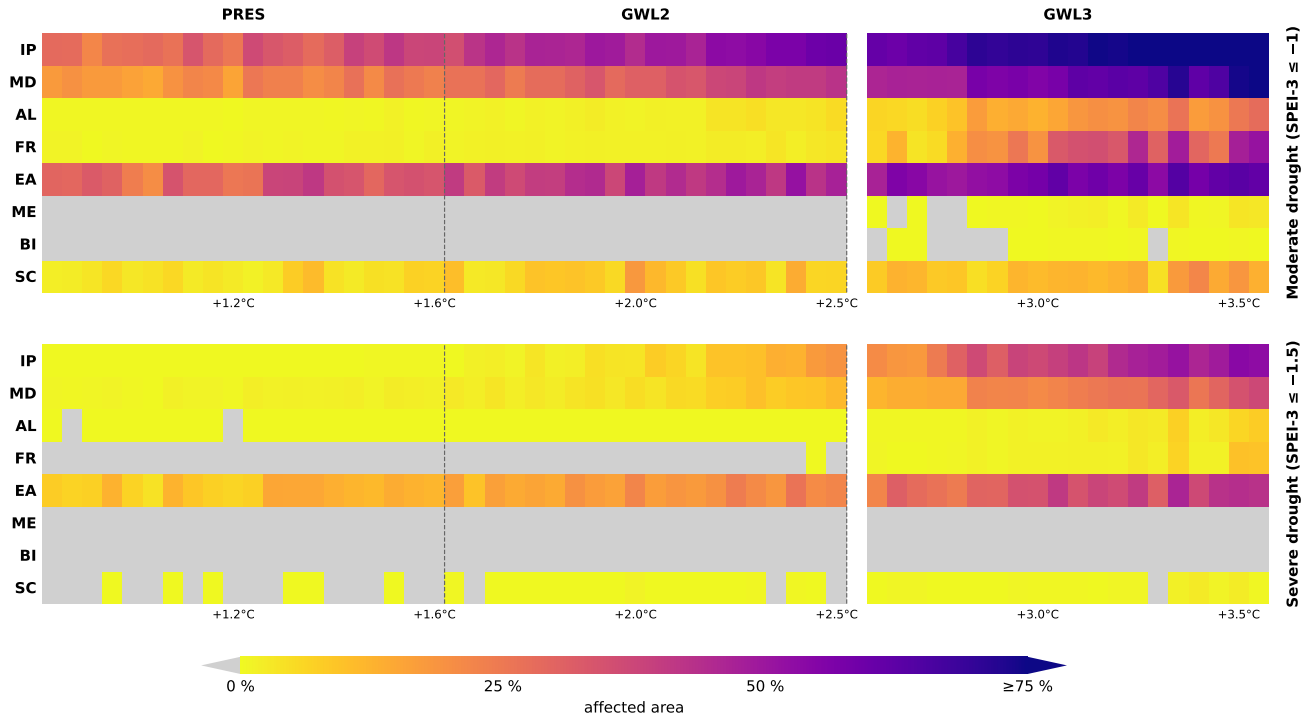

Figure 5. Minimum land surface fraction under near-certain drought exposure during late summer (JAS) by region. The colour of each tile encodes the minimum share of the regional land area exposed to drought, with grey representing 0%. The horizontal axis tracks the yearly global warming level. Moderate drought conditions are depicted in the top row and severe drought conditions in the bottom row.

late summer months and their transition into the wet season show an intensification of the drought signal, indicating recurring, longer, and more intense droughts. The late summer maximum and the lengthening of the dry season correspond to the July and August drought maxima reported for the same ensemble under a precipitation-only index [32].

Under global warming, drought variability increases specifically within drought hotspots. As a consequence, these regions can expect not only recurrent dry spells but also amplified extremes, including possibly unprecedented summer droughts.

The minimal expected signal of land area subject to drought conditions is increasing across the entire European continent under global warming. Eastern Europe already carries a drought signal under present conditions, largely induced by rising temperatures [32, 38]. The Iberian Peninsula, the Mediterranean, and Eastern Europe are most severely affected, with large areas of their territories certain to be affected by global warming. The Alpine domain and France show a specific response to +3 °C of global warming, in which the share of land with minimal drought coverage in late summer increases sharply.

All global warming levels show the same effect: under their respective best-case conditions, local drought persistence could be systematically delimited by orographic mountain lines, constraining northward and, to some extent, westward drought expansion [39]. On the other hand, even in a best-case scenario, the progression of moderate and severe drought alongside the Mediterranean coastline is almost certain. Under +3 °C of global warming, singular hotspots are certain to merge into a single European drought cover expanding across the entire southeastern Europe, where drought conditions with a yearly frequency must be expected even under an optimistic trajectory.

The persistence gradient in Figure 6, together with the variability in Figure 4, indicates locally stable drought conditions that are to be expected even under optimistic assumptions. The high and increasing variability means that unprecedentedly hot years are likely to occur, particularly in late summer. For agriculture, water supply and ecosystems across the Iberian Peninsula, the Mediterranean and Eastern Europe, this fraction marks the minimum that adaptation planning must already account for.

The near-certainty marks only where drought persists even under the wettest plausible conditions. Within the drought hotspots, a shift towards a drier state is near-certain under continued warming. The consequences might reach ecological systems, urban heat exposure, and the regional economy, including agriculture, water supply, energy, and public health [1]. Regions outside the hotspots may still require adaptation planning. Compared to +3 °C of global warming, the mean SPEI-3 signal and all variability-related consequences are essentially reduced under +2 °C.

Methods

We extend the aleatoric uncertainty decomposition of Gruber et al. [25], originally applied to water-balance variability over the Iberian Peninsula, to the European domain and propagate

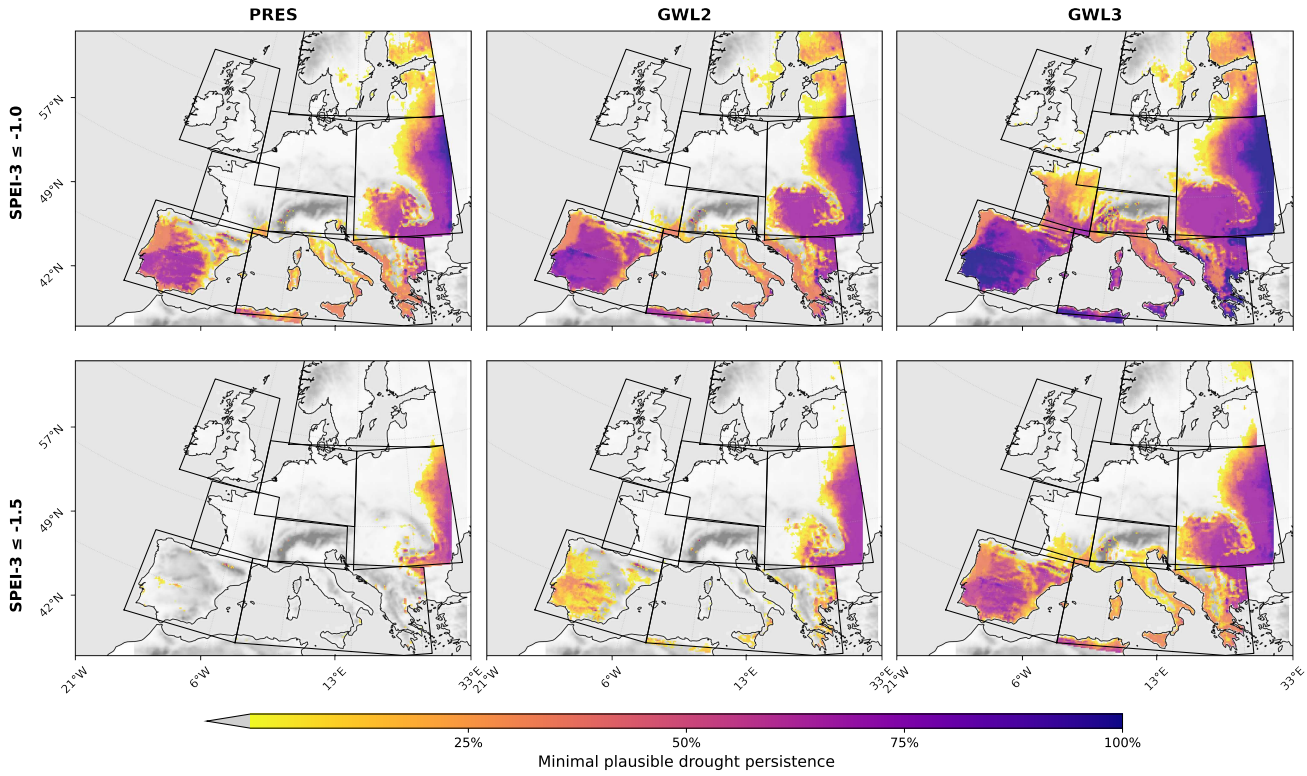

Figure 6. Evolution of regional hotspots of minimal plausible temporal *drought persistence* in late summer (JAS) under global warming. A frequency of 50% indicates that at least once every second late summer, a drought can be expected at the respective location. Columns facet across three GWL windows (PRES, GWL2, GWL3, left to right). The top row indicates the likelihood of moderate drought, and the bottom row indicates the likelihood of severe drought occurrence. Grey-shaded cells do not meet the criterion in any month but indicate elevations above the sea surface, illustrating the prominent role of topography as a boundary condition.

the resulting variability estimates through the SPEI transform to obtain drought bounds. The analysis targets SPEI-3. The three-month index aggregates the water balance of a meteorological season and is therefore the natural scale for the seasonal drought dynamics studied here.

Data

Climate model: CRCM5 large ensemble

We use the 50-member CRCM5 large ensemble [CRCM5-LE; 23, 40], a single-model initial-condition ensemble that dynamically downscales the CanESM2 global model over the EURO-CORDEX domain at 0.11° (about 12 km) resolution on the EUR-11 rotated-pole grid. The ensemble follows the RCP8.5 pathway from 2006 onward, and the analysis is organised by global warming level.

The members are organised into five families of ten perturbations each, which share identical physics and external forcing and differ only in initial conditions, forming an ensemble of equally plausible climate trajectories, ideal for quantifying internal variability [21, 22, 24, 41]. CRCM5-LE carries known precipitation and temperature biases (see Supplementary Figure 1) over parts of the domain [23]. The variability estimate is not affected by this bias by construction, because it is recovered from differences between members in which any shared bias cancels.

We limit our analyses of the CRCM5-LE to a maximum global warming of +3°C and use the global warming-level framing [1]. The GWLs are derived from the Canadian Earth System Model version 2, which provides the boundary conditions for CRCM5-LE. Using GWL instead of time horizons ensures comparability of this analysis across models and scenarios [29].

SPEI calibration from water balance

Monthly water balance is the difference between precipitation and potential evapotranspiration [42], $WB(s,t) = P(s,t) - PET(s,t)$, computed at each location s and month t for every CRCM5-LE member and for a reanalysis reference. For SPEI-3 we form three-month running sums

$$WB^{(3)}(s,t) = \sum_{u=0}^{2} WB(s,t-u). \qquad (1)$$

Accumulation precedes both standardisation and the variability decomposition.

ERA5-Land monthly reanalysis [43, 44] from 1971 to 2020 provides the calibration reference. The native grid is bilinearly interpolated to the EUR-11 rotated-pole grid with CDO [45] so that reference and model share spatial resolution. To transform water balance to the SPEI, we fit a three-parameter Gamma distribution (Pearson Type III)

[13, 46] to the monthly 50-year ERA5-Land $WB^{(3)}$ series, separately by grid cell, and transform any water-balance value through the fitted cumulative distribution and the standard-normal quantile function,

$$\text{SPEI-3}(x, s) = \Phi^{-1}\big(F_\Gamma(x;\, \hat\theta(s))\big)\,. \tag{2}$$

Gamma is preferred over the log-logistic and generalised extreme value distributions because their fits are not numerically stable across Europe's climatically diverse regimes, whereas the Gamma remains well-behaved. The transform yields an index on a common scale. Figure 1 indicates the present drought conditions in ERA5-Land. CRCM5-LE water balance is projected onto the ERA5-fitted parameters, so that shifts in SPEI between warming levels reflect changes to the historical water balance.

Consider the ensemble-mean water balance $\overline{WB}^{(3)}(s,t)$ as the expected seasonal water balance estimated over the 50 members, with the ensemble providing the plausible spread around it. The forced drought signal is the SPEI of this expectation,

$$\widetilde{\text{SPEI-3}}(s,t) = \Phi^{-1}\Big(F_\Gamma\Big(\overline{WB}^{(3)}(s,t);\, \hat\theta(s)\Big)\Big)\,. \tag{3}$$

Because SPEI is monotone but nonlinear, we transform $\overline{WB}^{(3)}$ such that the central estimate and the variability bounds (Equations 7 and 8) can be interpreted as mutually related quantities. SPEI is computed per grid cell over land cells only, and regional summaries are unweighted spatial means of the per-cell values after the transform, since cell area is approximately uniform on the EUR-11 rotated-pole grid.

Variability extraction

Internal variability is recovered from differences between members that share identical physics and forcing [25]. For two members i and j, the difference of their accumulated water-balance fields at the same (s,t) cancels the common mean state and bias components and isolates the internally generated variability, $\delta_{i,j}(s,t) = WB_i^{(3)}(s,t) - WB_j^{(3)}(s,t)$. Under the assumption of Gruber et al. [25] that the members share the same model bias and climatic mean state [23], are mutually independent, and share equal variance, and their variability has zero-mean [47, 48], the squared difference satisfies

$$\mathbb{E}\Big[\delta_{i,j}^2(s,t)\Big] = 2\,\sigma^2(s,t), \tag{4}$$

so modelling δ^2 yields a direct estimate of the internal variance. We use the within-family member pairs of CRCM5-LE following Gruber et al. [25].

The expected squared difference is modelled with a Gamma-family generalised additive model with log link [49],

$$\begin{aligned}\log \mu_{i,j}(s,t) = {}& \beta_0 + \beta_1\,\text{year} + f_1(\text{month}) \\ & + f_{\text{season}}(\text{lon},\text{lat}) + u_{i,j},\end{aligned} \tag{5}$$

where the year term is a within-window linear trend, f_1 is a cyclic cubic spline on calendar month, f_{season} is a season-specific tensor-product smooth on rotated longitude and latitude, and $u_{i,j}$ is a member-pair random intercept. Relative to Gruber et al. [25], the explicit elevation smooth is removed, because across the eight-region setting, elevation is largely collinear with the spatial smooth and is absorbed by $f_{\text{season}}(\text{lon},\text{lat})$. The internal variability is given by

$$\hat\sigma(s,t) = \sqrt{\tfrac{1}{2}\,\hat\mu_{i,j}(s,t)}. \tag{6}$$

Models are fitted with `bam` [mgcv; 49, 50] using fast restricted maximum likelihood and discretised covariates for scalability. One model is fitted per region and warming window, giving $8 \times 3 = 24$ fits. The variability is estimated directly on the three-month accumulated water balance. Further detail on the decomposition is given in Gruber et al. [25].

This formulation of internal variability has several advantages over window-based estimators [24, 23]. Variability is estimated as a continuous function of the covariate, so the amount of smoothing is chosen from the data by REML rather than fixed in advance by a 30-year window. Because the scale is a smooth of the forced state, ensembles are compared at equal warming levels. Changes in variability are read from the smooth and its derivative rather than from a reference-period variance test, whose outcome depends on the chosen baseline.

Two-sided variability bound

For each grid cell, month, and warming window, we construct a two-sided 95% variability interval on water balance around the ensemble mean, using the estimated standard deviation,

$$\begin{aligned} WB^L(s,t) &= \overline{WB}^{(3)}(s,t) - z_{0.975}\,\hat\sigma(s,t), \\ WB^U(s,t) &= \overline{WB}^{(3)}(s,t) + z_{0.975}\,\hat\sigma(s,t), \end{aligned} \tag{7}$$

with $z_{0.975} = 1.96$, the 97.5th quantile of the standard normal distribution. The Gaussian quantile is justified by the central limit theorem, given monthly aggregation and the ensemble sample size at each location. We use the climatic water balance rather than SPEI directly (see Supplementary Note).

Both values are mapped to SPEI through the ERA5-fitted Gamma distribution. Because F_Γ is monotone increasing, the transform preserves the quantiles,

$$\begin{aligned} \text{SPEI-3}^L(s,t) &= \Phi^{-1}\Big(F_\Gamma\Big(WB^L(s,t);\, \hat\theta(s)\Big)\Big), \\ \text{SPEI-3}^U(s,t) &= \Phi^{-1}\Big(F_\Gamma\Big(WB^U(s,t);\, \hat\theta(s)\Big)\Big). \end{aligned} \tag{8}$$

The triple $[\text{SPEI-3}^L,\ \widetilde{\text{SPEI-3}},\ \text{SPEI-3}^U]$ represents the drought-side tail, the forced signal, and the wet-side tail of the internal-variability distribution. SPEI-3^L characterises worst-case severity if variability acts against the mean, $\widetilde{\text{SPEI-3}}$ is the central estimate of the forced trajectory, and SPEI-3^U is the wet-side boundary that drives the near-certain hotspot criterion. Where even SPEI-3^U lies below a drought threshold, the forced signal is so dry that drought is near certain regardless of internal variability, which yields a conservative lower bound on the affected area.

Drought metrics and spatial aggregation

All maps use grid-cell SPEI-3 evaluated per calendar month and averaged into the four seasons, winter (DJF), spring (MAM), summer (JJA), and autumn (SON), or late summer (JAS) for display. Drought indications are reported at a moderate threshold $\tau = -1.0$ and the severe threshold $\tau = -1.5$.

Forced response: Figure 2 shows $\widetilde{\text{SPEI-3}}_{\text{PRES}}(s)$ and differences per warming level as

$$\Delta\widetilde{\text{SPEI-3}}(s) = \widetilde{\text{SPEI-3}}_{\text{GWL}}(s) - \widetilde{\text{SPEI-3}}_{\text{PRES}}(s). \quad (9)$$

Hatching marks areas where drought exposure can be expected $\widetilde{\text{SPEI-3}}(s) \leq -1.5$.

Variability ratio: Figure 4 shows the width of the two-sided SPEI-3 variability interval, $\text{SPEI-3}^U(s) - \text{SPEI-3}^L(s)$ and the ratio of this width between present conditions and GWL,

$$r(s) = \frac{\text{SPEI-3}^U_{\text{GWL}}(s) - \text{SPEI-3}^L_{\text{GWL}}(s)}{\text{SPEI-3}^U_{\text{PRES}}(s) - \text{SPEI-3}^L_{\text{PRES}}(s)}, \quad (10)$$

with $r(s) < 1$ for decreasing and $r(s) > 1$ for increasing variability.

Hotspot land fraction: Figure 5 and Table 1 define the near-certain drought fraction in late summer (JAS) for a region $\mathcal{R}$ as

$$A_\tau = \frac{1}{|\mathcal{R}|} \sum_{s \in \mathcal{R}} \mathbb{I}\left[\text{SPEI-3}^U(s) \leq \tau\right], \quad (11)$$

where $\mathbb{I}$ is an indicator function that accounts for whether even the *wet-side* bound SPEI-3^U at spatial coordinate s indicates a drought. $A_{-1.5} = 0.5$ means that, even under optimistic conditions, the climate model expects at least 50% of the area of region $\mathcal{R}$ under severe drought exposure. Figure 5 tracks the yearly global warming level and Table 1 the twenty-year window expected frequency, which are kept as distinct quantities.

Drought persistence: Figure 6 evaluates minimal plausible persistence as the fraction of late summers y in the respective period of global warming $\mathcal{Y}$,

$$F_\tau(s) = \frac{1}{|\mathcal{Y}|} \sum_{y \in \mathcal{Y}} \mathbb{I}\left[\text{SPEI-3}^U(s, y) \leq \tau\right], \quad (12)$$

So $F_{-1.5}(s) = 0.5$ means that a severe drought can be expected at least every second late summer. By "minimal plausible," we mean the wettest state that remains within the confidence interval. The counterpart worst-case scenario is depicted in Supplementary Figure 2.

Data availability

ERA5-Land reanalysis data are openly available from the Copernicus Climate Data Store at https://doi.org/10.24381/cds.68d2bb30 [43]. CRCM5-LE simulations for the historical and RCP8.5 scenarios are available from the ClimEx project [23] at https://www.climex-project.org/data-access/ on application. The processed outputs that support the findings of this study, comprising the calibration parameters of SPEI, the GAM fit, and the SPEI bound fields, are deposited on Zenodo at https://doi.org/10.5281/zenodo.20849199 and will be made openly available upon publication. During peer review, these outputs are available to the editors and reviewers on request.

Code availability

The analysis code and processing pipeline are openly available at the private repository https://github.com/henrifnk/spei_variability. The repository will be made openly available upon publication and is available to the editors and reviewers on request during peer review.

Acknowledgements

This research was supported by the DAAD programme Konrad Zuse Schools of Excellence in Artificial Intelligence, sponsored by the Federal Ministry of Research, Technology and Space, with no specific grant number available.

Author contributions

H.F. curated and prepared the climate model data, implemented the statistical modelling framework, performed the formal analysis and validation, produced the figures, and drafted the manuscript. H.F. and C.G. jointly developed the idea of linking internal climate variability to aleatoric uncertainty, bringing together uncertainty quantification and climate modelling. C.G. contributed to the methodology and to the review and editing of the manuscript. H.K. contributed to the statistical conceptualisation and methodology and co-supervised the project. M.M. supervised the project, and R.L. co-supervised it. Both contributed resources and domain expertise. A.B., A.S., and M.M. contributed domain knowledge and geographical expertise to the interpretation of the results and to the review and editing of the manuscript. All authors reviewed and approved the final manuscript.

Competing interests

The authors declare no competing interests.

References

[1] Intergovernmental Panel on Climate Change (IPCC). *Weather and Climate Extreme Events in a Changing Climate*, page 1513–1766. Cambridge University Press, 2023.

[2] C. Cammalleri, G. Naumann, L. Mentaschi, B. Bisselink, E. Gelati, A. De Roo, and L. Feyen. Diverging

hydrological drought traits over europe with global warming. *Hydrology and Earth System Sciences*, 24(12): 5919–5935, 2020. doi: 10.5194/hess-24-5919-2020. URL https://hess.copernicus.org/articles/24/5919/2020/.

[3] M. M. Vogel, J. Zscheischler, R. Wartenburger, D. Dee, and S. I. Seneviratne. Concurrent 2018 hot extremes across northern hemisphere due to human-induced climate change. *Earth's Future*, 7(7):692–703, 2019. doi: https://doi.org/10.1029/2019EF001189. URL https://agupubs.onlinelibrary.wiley.com/doi/abs/10.1029/2019EF001189.

[4] K. Stahl, I. Kohn, V. Blauhut, J. Urquijo, L. De Stefano, V. Acácio, S. Dias, J. H. Stagge, L. M. Tallaksen, E. Kampragou, A. F. Van Loon, L. J. Barker, L. A. Melsen, C. Bifulco, D. Musolino, A. de Carli, A. Massarutto, D. Assimacopoulos, and H. A. J. Van Lanen. Impacts of european drought events: insights from an international database of text-based reports. *Natural Hazards and Earth System Sciences*, 16(3):801–819, 2016. doi: 10.5194/nhess-16-801-2016. URL https://nhess.copernicus.org/articles/16/801/2016/.

[5] Jakob Zscheischler and Erich M. Fischer. The record-breaking compound hot and dry 2018 growing season in germany. *Weather and Climate Extremes*, 29:100270, 2020. ISSN 2212-0947. doi: https://doi.org/10.1016/j.wace.2020.100270. URL https://www.sciencedirect.com/science/article/pii/S2212094719302002.

[6] Emanuele Bevacqua, Oldrich Rakovec, Dominik L Schumacher, Rohini Kumar, Stephan Thober, Luis Samaniego, Sonia I Seneviratne, and Jakob Zscheischler. Direct and lagged climate change effects intensified the 2022 european drought. *Nature Geoscience*, 17(11): 1100–1107, 2024.

[7] Efi Rousi, Kai Kornhuber, Goratz Beobide-Arsuaga, Fei Luo, and Dim Coumou. Accelerated western european heatwave trends linked to more-persistent double jets over eurasia. *Nature communications*, 13(1):3851, 2022.

[8] Jonathan Spinoni, Jürgen V. Vogt, Gustavo Naumann, Paulo Barbosa, and Alessandro Dosio. Will drought events become more frequent and severe in europe? *International Journal of Climatology*, 38 (4):1718–1736, 2018. doi: https://doi.org/10.1002/joc.5291. URL https://rmets.onlinelibrary.wiley.com/doi/abs/10.1002/joc.5291.

[9] A. Böhnisch, E. Felsche, M. Mittermeier, B. Poschlod, and R. Ludwig. Future patterns of compound dry and hot summers and their link to soil moisture droughts in europe. *Earth's Future*, 13:e2024EF004916, 2025.

[10] Jakob Zscheischler, Olivia Martius, Seth Westra, Emanuele Bevacqua, Colin Raymond, Radley M Horton, Bart van den Hurk, Amir AghaKouchak, Aglaé Jézéquel, Miguel D Mahecha, et al. A typology of compound weather and climate events. *Nature reviews earth & environment*, 1(7):333–347, 2020.

[11] Yinglin Tian, Domenico Giaquinto, Giorgia Di Capua, Judith N Claassen, Javed Ali, Hao Li, and Carlo De Michele. Historical changes in the causal effect networks of compound hot and dry extremes in central europe. *Communications Earth & Environment*, 5(1): 764, 2024. doi: 10.1038/s43247-024-01934-2.

[12] Daniela IV Domeisen, Elfatih AB Eltahir, Erich M Fischer, Reto Knutti, Sarah E Perkins-Kirkpatrick, Christoph Schär, Sonia I Seneviratne, Antje Weisheimer, and Heini Wernli. Prediction and projection of heatwaves. *Nature Reviews Earth & Environment*, 4(1): 36–50, 2023.

[13] S. M. Vicente-Serrano, S. Begueria, and J. I. Lopez-Moreno. A multiscalar drought index sensitive to global warming: the spei. *Journal of Climate*, 23:1696–1718, 2010.

[14] James H Stagge, Daniel G Kingston, Lena M Tallaksen, and David M Hannah. Observed drought indices show increasing divergence across europe. *Scientific Reports*, 7(1):14045, 2017.

[15] Kunal Bhardwaj, Ashok Mishra, and C. Prakash Khedun. Global droughts in a warming climate: Evaluation of spi and spei under 1.5°, 2°, and 3°c global warming. *Journal of Hydrology*, 659:133309, 2025. ISSN 0022-1694. doi: https://doi.org/10.1016/j.jhydrol.2025.133309. URL https://www.sciencedirect.com/science/article/pii/S002216942500647X.

[16] Erasto Benedict Mukama, Estifanos Addisu Yimer, Winfred Baptist Mbungu, Stefaan Dondeyne, and Ann Van Griensven. Evaluating the standardized and threshold based drought indices for historical drought detection in the great ruaha river basin, tanzania. *Natural Hazards*, 121(10):12243–12273, 2025.

[17] E. Hawkins and R. Sutton. The potential to narrow uncertainty in regional climate predictions. *Bulletin of the American Meteorological Society*, 90:1095–1107, 2009.

[18] Ed Hawkins and Rowan Sutton. The potential to narrow uncertainty in projections of regional precipitation change. *Climate dynamics*, 37(1):407–418, 2011.

[19] F. Lehner, C. Deser, N. Maher, J. Marotzke, E. M. Fischer, L. Brunner, R. Knutti, and E. Hawkins. Partitioning climate projection uncertainty with multiple large ensembles and cmip5/6. *Earth System Dynamics*, 11(2):491–508, 2020. doi: 10.5194/esd-11-491-2020. URL https://esd.copernicus.org/articles/11/491/2020/.

[20] Goratz Beobide-Arsuaga, Laura Suarez-Gutierrez, Armineh Barkhordarian, Dirk Olonscheck, and Johanna

Baehr. Increasing central and northern european summer heatwave intensity due to forced changes in internal variability. *Nature Communications*, 16(1):9485, 2025.

[21] N. Maher, S. Milinski, and R. Ludwig. Large ensemble climate model simulations: introduction, overview, and future prospects for utilising multiple types of large ensemble. *Earth System Dynamics*, 12(2):401–418, 2021. doi: 10.5194/esd-12-401-2021. URL https://esd.copernicus.org/articles/12/401/2021/.

[22] C. Deser, F. Lehner, K. B. Rodgers, T. Ault, T. L. Delworth, P. N. DiNezio, A. Fiore, C. Frankignoul, J. C. Fyfe, D. E. Horton, J. E. Kay, R. Knutti, N. S. Lovenduski, J. Marotzke, K. A. McKinnon, S. Minobe, J. Randerson, J. A. Screen, I. R. Simpson, and M. Ting. Insights from earth system model initial-condition large ensembles and future prospects. *Nature Climate Change*, 10(4):277–286, April 2020. ISSN 1758-6798. doi: 10.1038/s41558-020-0731-2. URL https://www.nature.com/articles/s41558-020-0731-2. Publisher: Nature Publishing Group.

[23] M. Leduc et al. The ClimEx project: a 50-member ensemble of climate change simulations at 12-km resolution over europe and northeastern north america with the canadian regional climate model. *Journal of Applied Meteorology and Climatology*, 58:663–693, 2019.

[24] F. von Trentini, E. E. Aalbers, E. M. Fischer, and R. Ludwig. Comparing interannual variability in three regional single-model initial-condition large ensembles (smiles) over europe. *Earth System Dynamics*, 11(4):1013–1031, 2020. doi: 10.5194/esd-11-1013-2020. URL https://esd.copernicus.org/articles/11/1013/2020/.

[25] Cornelia Gruber, Henri Funk, Magdalena Mittermeier, Helmut Küchenhoff, and Göran Kauermann. Capturing aleatoric uncertainty in climate models. *Environmetrics*, 37(5):e70108, 2026. doi: https://doi.org/10.1002/env.70108. URL https://onlinelibrary.wiley.com/doi/abs/10.1002/env.70108.

[26] Cornelia Gruber, Patrick Oliver Schenk, Malte Schierholz, Frauke Kreuter, and Göran Kauermann. Sources of uncertainty in supervised machine learning – a statisticians' view, 2025. URL https://arxiv.org/abs/2305.16703.

[27] Eyke Hüllermeier and Willem Waegeman. Aleatoric and epistemic uncertainty in machine learning: An introduction to concepts and methods. *Machine learning*, 110(3):457–506, 2021.

[28] Jens Hesselbjerg Christensen and Ole Bøssing Christensen. A summary of the prudence model projections of changes in european climate by the end of this century. *Climatic change*, 81(Suppl 1):7–30, 2007.

[29] D. Gampe, C. Schwingshackl, A. Böhnisch, M. Mittermeier, M. Sandstad, and R. R. Wood. Applying global warming levels of emergence to highlight the increasing population exposure to temperature and precipitation extremes. *Earth System Dynamics*, 15(3):589–605, 2024. doi: 10.5194/esd-15-589-2024. URL https://esd.copernicus.org/articles/15/589/2024/.

[30] Elizaveta Felsche, Andrea Böhnisch, Benjamin Poschlod, and Ralf Ludwig. European hot and dry summers are projected to become more frequent and expand northwards. *Communications Earth & Environment*, 5(1):410, 2024.

[31] J. Cos, F. Doblas-Reyes, M. Jury, R. Marcos, P.-A. Bretonnière, and M. Samsó. The mediterranean climate change hotspot in the cmip5 and cmip6 projections. *Earth System Dynamics*, 13(1):321–340, 2022. doi: 10.5194/esd-13-321-2022. URL https://esd.copernicus.org/articles/13/321/2022/.

[32] Andrea Böhnisch, Magdalena Mittermeier, Martin Leduc, and Ralf Ludwig. Hot spots and climate trends of meteorological droughts in europe–assessing the percent of normal index in a single-model initial-condition large ensemble. *Frontiers in Water*, Volume 3 - 2021, 2021. ISSN 2624-9375. doi: 10.3389/frwa.2021.716621. URL https://www.frontiersin.org/journals/water/articles/10.3389/frwa.2021.716621.

[33] Nikolaus Obojes, Armin Meurer, Christian Newesely, Erich Tasser, Walter Oberhuber, Stefan Mayr, and Ulrike Tappeiner. Water stress limits transpiration and growth of european larch up to the lower subalpine belt in an inner-alpine dry valley. *The New Phytologist*, 220(2):460, 2018.

[34] L. Samaniego et al. Anthropogenic warming exacerbates european soil moisture droughts. *Nature Climate Change*, 8:421–426, 2018.

[35] Vittal Hari, Oldrich Rakovec, Yannis Markonis, Martin Hanel, and Rohini Kumar. Increased future occurrences of the exceptional 2018–2019 central european drought under global warming. *Scientific reports*, 10(1):12207, 2020.

[36] J. Ignacio López-Moreno and Sergio M. Vicente-Serrano. Positive and negative phases of the wintertime north atlantic oscillation and drought occurrence over europe: A multitemporal-scale approach. *Journal of Climate*, 21(6):1220 – 1243, 2008. doi: 10.1175/2007JCLI1739.1. URL https://journals.ametsoc.org/view/journals/clim/21/6/2007jcli1739.1.xml.

[37] Ileana Bladé, Brant Liebmann, Didac Fortuny, and Geert Jan van Oldenborgh. Observed and simulated impacts of the summer nao in europe: implications for projected drying in the mediterranean region. *Climate dynamics*, 39(3):709–727, 2012.

[38] M. Ionita and V. Nagavciuc. Changes in drought features at the european level over the last 120 years. *Natural Hazards and Earth System Sciences*, 21(5):1685–1701, 2021. doi: 10.5194/nhess-21-1685-2021. URL https://nhess.copernicus.org/articles/21/1685/2021/.

[39] Andreas Gobiet, Sven Kotlarski, Martin Beniston, Georg Heinrich, Jan Rajczak, and Markus Stoffel. 21st century climate change in the european alps—a review. *Science of The Total Environment*, 493:1138–1151, 2014. ISSN 0048-9697. doi: https://doi.org/10.1016/j.scitotenv.2013.07.050. URL https://www.sciencedirect.com/science/article/pii/S0048969713008188.

[40] Leo Šeparović, Adelina Alexandru, René Laprise, Andrey Martynov, Laxmi Sushama, Katja Winger, Kossivi Tete, and Michel Valin. Present climate and climate change over north america as simulated by the fifth-generation canadian regional climate model. *Climate Dynamics*, 41(11):3167–3201, 2013.

[41] J. E. Kay, C. Deser, A. Phillips, A. Mai, C. Hannay, G. Strand, J. M. Arblaster, S. C. Bates, G. Danabasoglu, J. Edwards, M. Holland, P. Kushner, J.-F. Lamarque, D. Lawrence, K. Lindsay, A. Middleton, E. Munoz, R. Neale, K. Oleson, L. Polvani, and M. Vertenstein. The Community Earth System Model (CESM) Large Ensemble Project: A Community Resource for Studying Climate Change in the Presence of Internal Climate Variability. *Bulletin of the American Meteorological Society*, 96(8):1333–1349, August 2015. ISSN 0003-0007, 1520-0477. doi: 10.1175/BAMS-D-13-00255.1.

[42] Charles Warren Thornthwaite. An approach toward a rational classification of climate. *Geographical review*, 38(1):55–94, 1948.

[43] Joaquín Muñoz-Sabater, Emanuel Dutra, Anna Agustí-Panareda, Clément Albergel, Gabriele Arduini, Gianpaolo Balsamo, Souhail Boussetta, Margarita Choulga, Shaun Harrigan, Hans Hersbach, et al. Era5-land: A state-of-the-art global reanalysis dataset for land applications. *Earth system science data*, 13(9):4349–4383, 2021.

[44] Hans Hersbach, Bill Bell, Paul Berrisford, Shoji Hirahara, András Horányi, Joaquín Muñoz-Sabater, Julien Nicolas, Carole Peubey, Raluca Radu, Dinand Schepers, Adrian Simmons, Cornel Soci, Saleh Abdalla, Xavier Abellan, Gianpaolo Balsamo, Peter Bechtold, Gionata Biavati, Jean Bidlot, Massimo Bonavita, Giovanna De Chiara, Per Dahlgren, Dick Dee, Michail Diamantakis, Rossana Dragani, Johannes Flemming, Richard Forbes, Manuel Fuentes, Alan Geer, Leo Haimberger, Sean Healy, Robin J. Hogan, Elías Hólm, Marta Janisková, Sarah Keeley, Patrick Laloyaux, Philippe Lopez, Cristina Lupu, Gabor Radnoti, Patricia de Rosnay, Iryna Rozum, Freja Vamborg, Sebastien Villaume, and Jean-Noël Thépaut. The ERA5 global reanalysis. *Quarterly Journal of the Royal Meteorological Society*, 146 (730):1999–2049, 2020. ISSN 1477-870X. doi: 10.1002/qj.3803. URL https://onlinelibrary.wiley.com/doi/abs/10.1002/qj.3803. _eprint: https://rmets.onlinelibrary.wiley.com/doi/pdf/10.1002/qj.3803.

[45] Uwe Schulzweida. Cdo user guide, October 2023. URL https://doi.org/10.5281/zenodo.10020800.

[46] James H. Stagge, Lena M. Tallaksen, Lukas Gudmundsson, Anne F. Van Loon, and Kerstin Stahl. Candidate distributions for climatological drought indices (spi and spei). *International Journal of Climatology*, 35 (13):4027–4040, 2015. doi: https://doi.org/10.1002/joc.4267. URL https://rmets.onlinelibrary.wiley.com/doi/abs/10.1002/joc.4267.

[47] David W. J. Thompson, Elizabeth A. Barnes, Clara Deser, William E. Foust, and Adam S. Phillips. Quantifying the Role of Internal Climate Variability in Future Climate Trends. *Journal of Climate*, 28(16):6443–6456, August 2015. ISSN 0894-8755, 1520-0442. doi: 10.1175/JCLI-D-14-00830.1.

[48] Ram Singh and K. AchutaRao. Quantifying uncertainty in twenty-first century climate change over India. *Climate Dynamics*, 52(7):3905–3928, April 2019. ISSN 1432-0894. doi: 10.1007/s00382-018-4361-6.

[49] S. N. Wood. *Generalized Additive Models: An Introduction with R*. Chapman and Hall/CRC, Boca Raton, 2nd edition, 2017.

[50] S. N. Wood, Y. Goude, and S. Shaw. Generalized additive models for large data sets. *Journal of the Royal Statistical Society Series C*, 64:139–155, 2015.

Supplementary Files

This is a list of supplementary files associated with this preprint. Click to download.

- SPEIVariabilityPreprintSupp.pdf